# Spatial Interpolation of Daily Precipitation in a High Mountainous Watershed Based on Gauge Observations and a Regional Climate Model Simulation

YUHAN WANG, HANBO YANG, DAWEN YANG, AND YUE QIN

*State Key Laboratory of Hydroscience and Engineering, Department of Hydraulic Engineering, Tsinghua University, Beijing, China*

BING GAO

*School of Water Resources and Environment, China University of Geosciences, Beijing, China*

ZHENTAO CONG

*State Key Laboratory of Hydroscience and Engineering, Department of Hydraulic Engineering, Tsinghua University, Beijing, China*

(Manuscript received 9 April 2016, in final form 25 November 2016)

ABSTRACT

Precipitation is a primary climate forcing factor in catchment hydrology, and its spatial distribution is essential for understanding the spatial variability of ecohydrological processes in a catchment. In mountainous areas, meteorological stations are generally too sparse to represent the spatial distribution of precipitation. This study develops a spatial interpolation method that combines meteorological observations and regional climate model (RCM) outputs. The method considers the precipitation–elevation relationship in the mountain region and the topographic effects, especially the mountain blocking effect. Furthermore, using this method, this study produced a 3-km-resolution precipitation dataset from 1960 to 2014 in the middle and upper reaches of the Heihe River basin located on the northern slope of the Qilian Mountains in the northeastern Tibetan Plateau. Cross validation based on the station observations showed that this method is reasonable. The rationality of the interpolated precipitation data was also evaluated by the catchment water balances using the observed river discharge and the actual evapotranspiration based on remote sensing. The interpolated precipitation data were compared with the China Gauge-Based Daily Precipitation Analysis product and the RCM output and was shown to be optimal. The results showed that the proposed method effectively used the information from the meteorological observations and the RCM simulations and provided the spatial distributions of daily precipitations with reasonable accuracy and high resolution, which is important for a distributed hydrological simulation at the catchment scale.

## 1. Introduction

Precipitation is the primary driver of the ecohydrological processes in a watershed (Z. Li et al. 2013; Kaptué et al. 2015). Because precipitation influences the spatial organization of runoff, evaporation, and soil moisture, consequently affecting the ecological process (Taylor et al. 1997; Nykanen et al. 2001), the spatial distribution of precipitation is important for understanding the spatial characteristics of ecohydrology at the watershedvscale.

Different spatial interpolation techniques are used to obtain gridded precipitation data based on gauge observations (Tabios and Salas 1985), including the widely used Thiessen polygon (Thiessen 1911), the methods of Inverse Distance Weighting (IDW; Shepard 1968) and Angular Distance Weighting (ADW; Willmott et al. 1985), and the splines (Hutchinson 1995) and kriging techniques (Phillips et al. 1992). A common feature of these methods is the estimation of grid precipitation as the weighted average of the relevant gauge observations (Willmott and Matsuura 1995); the difference among these techniques is the method used for calculating the weight of each precipitation gauge. Precipitation is often affected by terrain changes (Basist

*Corresponding author e-mail*: Dawen Yang, yangdw@tsinghua.edu.cn

DOI: 10.1175/JHM-D-16-0089.1

et al. 1994; Lloyd 2005). In mountainous areas, precipitation on the top of the mountain may be significantly different from the precipitation at the foot of the mountain (Sanberg and Oerlemans 1983; Daly et al. 2008). Daly et al. (1994) did several studies on the relationship between precipitation and topography uplift, and proposed a linear precipitation–elevation relationship. In high mountainous watersheds, there are few meteorological stations located at high elevations; the precipitation interpolation based on the stations at low elevations is often unrepresentative at high elevations (Daly et al. 2008). This is a common problem for precipitation interpolation based on the sparse observations in mountainous regions. To obtain the spatial distribution of precipitation in mountainous regions, information about the precipitation spatial pattern/characteristics affected by the terrain is required.

To consider the effect of the terrain on precipitation, interpolation methods such as kriging or splines have added the elevation element (New et al. 1999, 2000). Daly et al. (1994) developed a method that uses a local regression technique to consider the effect of terrain, called the Parameter-Elevation Regressions on Independent Slopes Model (PRISM). In this method, the key step is estimating the precipitation–elevation relationship, which is the basis for the annual or monthly precipitation interpolation. To estimate the precipitation–elevation relationship, the terrain is smoothed and divided into the east-, south-, west-, and north-oriented (or flat) slope facets. In each facet, the precipitation–elevation regression function is developed based on the station precipitation data, and the precipitation–elevation gradient is generated. Xie et al. (2007) developed a daily precipitation interpolation method using PRISM. This method estimates the gridded daily precipitation based on the station observations using the precipitation–elevation relationship estimated by PRISM. Using this method, a dataset of daily precipitation with a spatial resolution of 0.25° over the mainland of China is generated from the observations of 2400 meteorological stations; these data are called the China Gauge-Based Daily Precipitation Analysis (CGDPA) product (Shen and Xiong 2016). Remarkably, PRISM relies on the precipitation–elevation relationship for each facet that was estimated according to the gauge measurements. To obtain precise high spatial precipitation values, a sufficient number of gauges in each facet is required. Unfortunately, gauges are generally sparse in mountainous areas.

Currently, there are two primary types of precipitation products, satellite observation precipitation and radar observation precipitation, which can provide the spatial distribution of precipitation (Berne and Krajewski 2013). However, because of the low spatial resolution, satellite precipitation products, such as TRMM (Huffman et al. 2007) and CMORPH (Joyce et al. 2004), are often unable to meet the demand in many ecohydrological models with high spatial resolution (Hofstra et al. 2008). Radar precipitation observations often have large uncertainties in mountainous areas because of the interference of complex terrain in radar observations (Young et al. 1999; Li et al. 2014); in addition, there are no radar observations in many mountainous areas.

Regional climate models (RCM) can provide the output of meteorological elements, including precipitation, with a high spatial resolution (Diallo et al. 2012). RCMs utilize the output from global climate models (GCMs) as the lateral boundary conditions (Dickinson et al. 1989; Giorgi and Bates 1989) and downscale the GCM output to the regional scale based on the physical processes and local features (such as atmospheric dynamics, local topography, and vegetation cover). RCMs have been applied and intensively evaluated in different regions of the world in previous studies (Liang et al. 2004; Maurya and Singh 2016; Maraun and Widmann 2015). RCMs provide valuable information about the spatial distribution of precipitation (Xiong et al. 2009; Xiong and Yan 2013; Laux et al. 2011; Feldmann et al. 2013) that is potentially useful for the interpolation of gauge precipitation measurements.

Therefore, this study aims to develop an interpolation method for the gauge-sparse mountainous area by utilizing the spatial distribution information provided by the RCM output with fine spatial resolution and to apply this method to the middle and upper reaches of the Heihe River basin to generate high-resolution gridded data of daily precipitation from 1960 to 2014. The interpolation method is introduced in detail in section 2. Application to the Heihe River basin is presented in section 3, which includes the introduction of the study area and the data description. In section 4, the method validation is presented, followed by a comparison of the interpolation result with other precipitation datasets; furthermore, the rationality of the precipitation interpolation is evaluated using water balance analysis. Finally, the conclusions are listed in section 5.

## 2. Interpolation method

The primary steps of the interpolation method can be described as follows. The first and most important step is to generate the gridded daily climatological precipitation, which represents the spatial distribution of long-term mean daily precipitation. The second step is to calculate the gridded ratio of daily precipitation to the daily climatological precipitation by interpolating the ratio values at the stations. Finally, gridded daily precipitation is

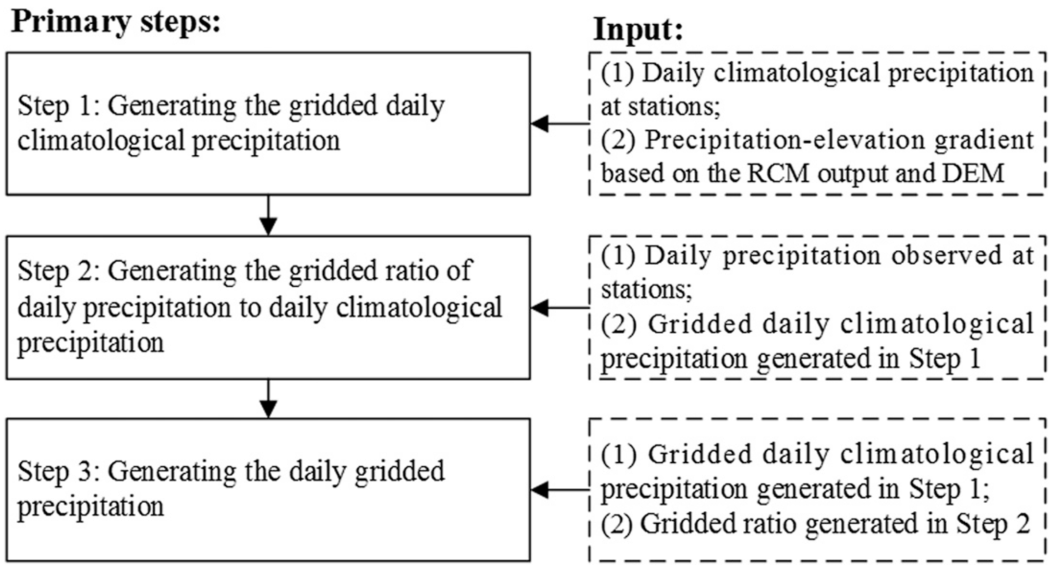


FIG. 1. Primary steps of the interpolation method.

estimated as the product of the daily climatological precipitation and the daily precipitation ratio. Figure 1 shows the diagram of the proposed method.

### a. *Generating the gridded daily climatological precipitation*

The stations provide accurate precipitation values at a point scale, while the RCM provides gridded precipitation data from which the spatial distribution pattern of precipitation can be extracted. Therefore, the gridded daily climatological precipitation is generated by merging a station's daily climatological precipitation and the spatial distribution characteristics estimated from the RCM output.

The station's daily climatological precipitation is defined as the mean daily precipitation for each day of year (DOY), which is calculated from long-term daily precipitation observed at stations. The long-term mean daily precipitation for the 365 calendar days is calculated at each station, and then a smooth curve of the long-term mean daily precipitation is obtained and the high-frequency noise is removed using the Fourier filtering process. The filtering result is considered the daily climatological precipitation (see Fig. A1 in the appendix for details).

The precipitation–elevation relationship at the monthly time scale is estimated from RCM output and is used to represent the spatial distribution characteristics of the precipitation in the mountainous areas. To estimate the precipitation–elevation relationship, three steps are taken as follows.

The first step is to divide the entire terrain into facets. This study uses a digital elevation model (DEM) with the same projection and resolution as the RCM. Based on the DEM, the entire terrain is divided into facets. The adjacent grid cells with the same major orientation (east, south, west, north, or flat) are grouped into one facet. However, the facets derived from the DEM are probably fragmentary, and thus a smoothing process is applied. In the smoothing process, the elevation of each grid cell in the DEM is updated as follows:

$$\begin{aligned} \mathrm{ele}_{m,n} &= 0.5\mathrm{ele}_{m,n} + 0.125(\mathrm{ele}_{m-1,n} + \mathrm{ele}_{m+1,n} \\ &\quad + \mathrm{ele}_{m,n-1} + \mathrm{ele}_{m,n+1}), \end{aligned} \tag{1}$$

where $\mathrm{ele}_{m,n}$ is the elevation of the grid cell at row $m$ and column $n$. Repeating this smoothing process using Eq. (1), the terrain of the entire study area is smoothed to contain the major graphical features. As suggested by Daly et al. (1994), multiple-of-8 cycles of the smoothing process [8, 16, 24, 32, 40 repeated cycles of Eq. (1)] are performed. By judging the number of the fragment facets that contain five or fewer grid cells and the distortion degree of the terrain, the most suitable terrain after certain cycles of the smoothing process is selected.

The second step is to estimate the precipitation–elevation gradient in each facet using a regression analysis based on the RCM monthly precipitation. The regression is performed in a facet that contains more than five grid cells. In the remaining facets, which contain five or fewer grids, the precipitation–elevation gradient is calculated as the mean values of the surrounding facets.

The third step is to adjust the precipitation–elevation gradient according to station observations. A bias may exist in the absolute value of the precipitation–elevation gradient calculated from the RCM output, and it can be adjusted according to the station observations. The mean precipitation–elevation gradient for the entire mountain area is estimated from the RCM output and the station observations, denoted $G_R$ and $G_s$, respectively. The ratio of $G_R$ and $G_s$ is used to correct the systematic bias of the precipitation–elevation gradient estimated from the RCM output in each facet. The gradient value is estimated in the monthly scale, and it is assumed that the daily gradients in a month have the same value.

Based on the climatological precipitation at stations and the precipitation–elevation gradient, the gridded daily climatological precipitation is interpolated. The interpolation method used in this study is a modified ADW (Willmott et al. 1985; New et al. 2000; Yang et al. 2004) with a consideration of the precipitation–elevation gradient. To interpolate the daily climatological precipitation at a grid cell $(m, n)$ $P_{\mathrm{cli}(m,n)}$, the nearest stations within a distance of $x_0$ centered at the target grid cell (up to eight stations) are selected, and $x_0$ is a correlation decay distance with a range of 350–500 km (New et al. 2000). The distance weight for the station $i$ is calculated as follows:

$$w_{0(m,n),i} = (e^{-x/x_0})^t, \tag{2}$$

where $x$ is the distance from the target grid cell $(m, n)$ to the station $i$, $x_0$ is the correlation decay distance ($x_0$ = 500 km), and $t$ is an adjustable parameter (usually set to 4; New et al. 2000). The distance weight is adjusted according to the relative direction among the stations. The adjustment coefficient $a_{(m,n),i}$ is calculated as follows:

$$a_{(m,n),i} = \frac{\sum_{l=1}^{\mathrm{nos}} w_{0(m,n),l}[1 - \cos\theta_{m,n}(i,l)]}{\sum_{l=1}^{\mathrm{nos}} w_{0(m,n),l}}, \quad l \neq i, \tag{3}$$

where $\theta_{m,n}(i, l)$ is the separate angle of stations $i$ and $l$ to the target grid cell $(m, n)$, $w_{0(m,n),l}$ is the distance weight of station $l$, and nos is the number of stations used to interpolate the target grid cell $(m, n)$. The angular distance weight is finally modified as follows:

$$w_{(m,n),i} = w_{0(m,n),i}[1 + a_{(m,n),i}]. \tag{4}$$

Then, the daily climatological precipitation of the grid cell at row $m$ and column $n$ [i.e., $P_{\mathrm{cli}(m,n)}$] is calculated as follows:

$$P_{\mathrm{cli}(m,n)} = \left\{ \sum_{i=1}^{\mathrm{nos}} w_{(m,n),i} \times [P_{\mathrm{cli},i} + \overline{S}_{(m,n),i} \times (\mathrm{ele}_{m,n} - \mathrm{ele}_i)] \right\} \bigg/ \sum_{i=1}^{\mathrm{nos}} w_{(m,n),i}, \tag{5}$$

where $P_{\mathrm{cli},i}$ is the daily climatological precipitation at the $i$th station; $\mathrm{ele}_{m,n}$ is the elevation of the target grid cell; $\mathrm{ele}_i$ is the elevation of the $i$th station; and $\overline{S}_{(m,n),i}$ is the average precipitation–elevation slope between the $i$th station and the target grid cell $(m, n)$, which is estimated as follows:

$$\overline{S}_{(m,n),i} = \left\{ \sum_{j=1}^{\mathrm{nog}-1} [\mathrm{grad}_j \times (\mathrm{ele}_{j+1} - \mathrm{ele}_j)] \right\} \bigg/ (\mathrm{ele}_{m,n} - \mathrm{ele}_i), \tag{6}$$

where nog is the number of grid cells located along the direction from the $i$th station to the target grid cell $(m, n)$; $j$ is the serial number of the nos grid cells, where the grid cell with $j$ equal to 1 is the grid cell where the $i$th station is located and the grid cell with $j$ equal to nog is the target grid cell $(m, n)$; and $\mathrm{grad}_j$ is the gradient value of the facet where the $j$th grid is located.

### b. *Interpolating the ratio of the daily precipitation to the daily climatological precipitation from the station to the grid*

First, the ratio of the daily precipitation to the daily climatological precipitation is estimated at each station as follows:

$$\mathrm{ratio}_i = \frac{P_i}{P_{\mathrm{cli},i}}, \tag{7}$$

where $P_i$ is the daily precipitation at station $i$ and $P_{\mathrm{cli},i}$ is the daily climatological precipitation at station $i$. Then, we interpolate the ratios at the stations into gridded ratios with the same spatial resolution of the gridded climatological precipitation using the ADW method.

During the ratio interpolation, the mountain blocking effect on precipitation is considered. The precipitation is larger on the upwind side of the mountain than that on the opposite side. When a grid cell $(m, n)$ is being interpolated, the weight of the stations located in the same side of the mountain as the target grid is increased as follows:

$$\mu_{(m,n),i} = \beta \times w_{(m,n),i}, \tag{8}$$

where $\mu_{(m,n),i}$ is the adjusted weight considering the mountain blocking effect; $w_{(m,n),i}$ is the original weight of the $i$th station calculated by Eqs. (2)–(4); and $\beta$ is an adjusting coefficient, which is larger than 1. The value of $\beta$ is determined according to the coefficient of determination $R^2$ of the generalized cross validation (GCV) result (Willmott and Matsuura 1995). In the GCV process, each station is used to validate the interpolation result from the other stations. A different value of $\beta$ generates a different GCV result (i.e., $R^2$), and the average value of $R^2$ for all stations is calculated. The appropriate value of $\beta$ is selected, which corresponds to the maximum $R^2$. For the stations located on the different side of the mountain as the target grid, $\mu_{(m,n),i}$ is equal to $w_{(m,n),i}$.

After the weight is adjusted, the ratio of the grid cell at row $m$ and column $n$ is calculated as follows:

$$\text{ratio}_{m,n} = \left[\sum_{i=1}^{\text{nos}} \mu_{(m,n),i} \times \text{ratio}_i\right] \Big/ \sum_{i=1}^{\text{nos}} \mu_{(m,n),i}, \qquad (9)$$

where nos is the number of stations within a distance of 500 km (up to eight stations are used), $\text{ratio}_i$ is the daily ratio value at the $i$th station of the number of stations, and $\mu_{(m,n),i}$ is the adjusted weight of the $i$th station.

The ADW method may cause false precipitation. Thus, the ratio should be adjusted using a rain/no-rain discrimination. In this study, a threshold parameter $\alpha$ is adapted, and the original ratio in each grid (i.e., $\text{ratio}_{m,n}$) is adjusted as follows:

$$\begin{cases} \text{ratio}'_{m,n} = 0 \left[\text{ratio}_{m,n} < \min\limits_{i=1}^{k} (\alpha \times \text{ratio}_i)\right] \\ \text{ratio}'_{m,n} = \text{ratio}_{m,n} (\text{ in other cases}) \end{cases}, \qquad (10)$$

where $\text{ratio}'_{m,n}$ is the adjusted ratio of the grid cell $(m, n)$, $k$ is the number of show-precipitation stations in the nos utilized to interpolate the grid precipitation (the ratios in these $k$ stations are greater than 0), and $\text{ratio}_i$ is the ratio value at the $i$th station of the $k$ stations. The parameter $\alpha$ ranges from 0 to 1 and is determined according to the false alarms and misses of the interpolation precipitation.

### c. *Generating the daily gridded precipitation*

Finally, the daily gridded precipitation is calculated by multiplying the daily climatological precipitation by the daily ratio. The daily precipitation of the grid cell at row $m$ and column $n$ (i.e., $P_{m,n}$) is estimated as follows:

$$P_{m,n} = P_{\text{cli}(m,n)} \times \text{ratio}'_{m,n} \qquad (11)$$

where $P_{\text{cli}(m,n)}$ is the daily climatological precipitation in grid $(m, n)$, which is calculated using Eq. (5); $\text{ratio}'_{m,n}$ and is the adjusted daily ratio value for grid cell $(m, n)$, which is calculated using Eq. (9) first and then adjusted using Eq. (10).

## 3. Application to the Heihe River basin

### a. *Study area*

The Heihe River basin (HRB) is the second-largest inland river basin in China; it originates from the northern slope of the Qilian Mountains located in the northeastern Tibetan Plateau, flows through the Hexi Corridor, and ends in Ju Yanhai Lake (Fig. 2). The precipitation in the HRB has a highly spatial and temporal variability (Xiong and Yan 2013; Pan et al. 2015). The upper reach has an abundant precipitation amount of approximately 700–200 mm yr$^{-1}$, while in the middle and lower reaches the annual precipitation is only approximately 200–50 mm. For the annual precipitation distribution, nearly 60% of the annual precipitation falls in the summer from June to September (Ding et al. 1999; Gao et al. 2016). The upper reaches located in the Qilian Mountains with an elevation above 1700 m are the source areas that supply the water resources to the middle reaches for social economic development and to the downstream area for sustaining the ecosystem (Yang et al. 2015; Gao et al. 2016).

The upper reaches of the Heihe River consist of several subbasins. The largest subbasin located in the east, which is gauged at the Yingluoxia hydrological station, has a drainage area of 10 009 km$^2$ and generates nearly 70% of the basin's total runoff (Yang et al. 2015). After

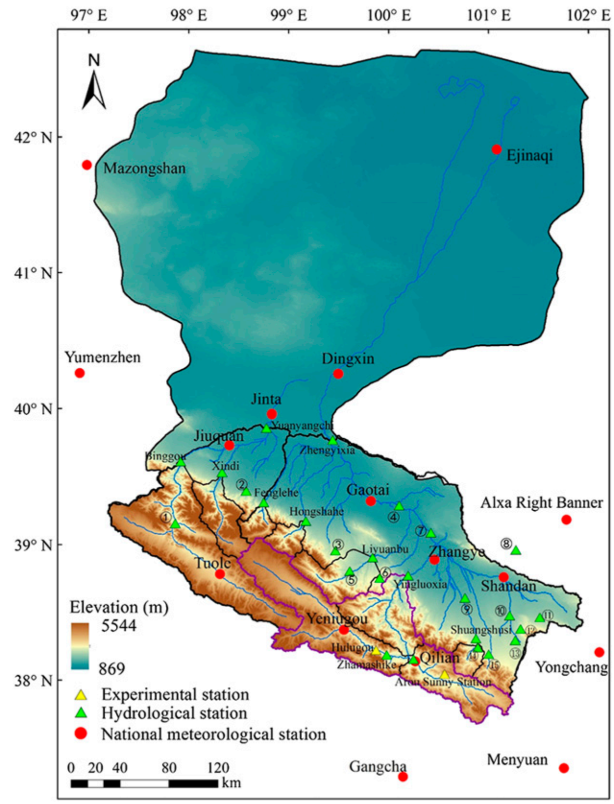


FIG. 2. Study area and locations of hydrological stations, meteorological stations, and experimental stations. The names of the hydrological stations identified by numbers are 1) Zhulongguan, 2) Hongshan, 3) Dahe, 4) Pingchuan, 5) Sunan, 6) Kangle, 7) Gaoya, 8) Hongsihu, 9) Liuba, 10) Liqiao, 11) Xiakouyi, 12) Dahuangshan, 13) Maying, 14) Binggoutai, and 15) Biandukou.

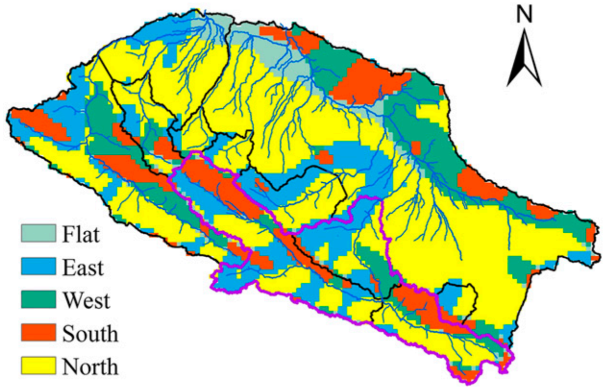


FIG. 3. The division of facets according to the main slope direction based on the DEM after 16 times cycles of smooth processing, a total of 61 facets.

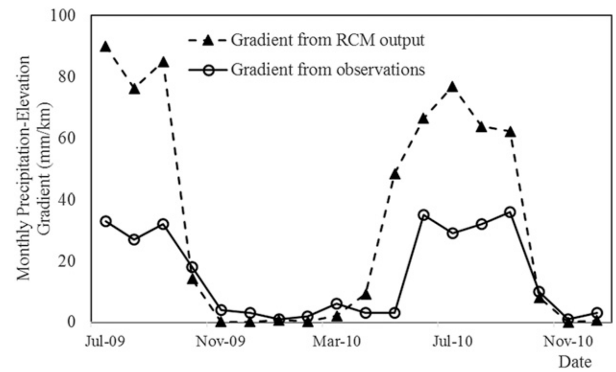


FIG. 5. Monthly precipitation–elevation gradient derived from the RCM output and the observations in the Hulugou experimental catchment.

the Yingluoxia station, the main river flows through the Zhangye Plain and finally flows downstream via the Zhengyixia station. In addition to the main stream, another major subbasin is the Beidahe River in the west; its upstream has a drainage area of 6966 $km^2$ at the Bingou hydrological station. This tributary flows to the middle stream via the Binggou station and, finally, to the downstream via the Yuanyangchi station. In addition, small mountain rivers flow into the main stream or Beidahe River (Fig. 2).

### b. Data used

The data used in this study include DEM data and precipitation data. The DEM data are obtained from the SRTM database (Jarvis et al. 2008). Precipitation data include gauge precipitation data and the RCM simulation result.

#### 1) GAUGE PRECIPITATION DATA

The gauge data used in this study are the daily precipitation values observed at 15 national meteorological stations and 25 hydrological stations in the upper and middle reaches of the HRB. The national meteorological stations record the meteorological elements of precipitation, air temperature, relative humidity, sunshine hours, pan evaporation, atmospheric pressure, and wind speed. The daily data are obtained from the China Meteorological Data Sharing Service System

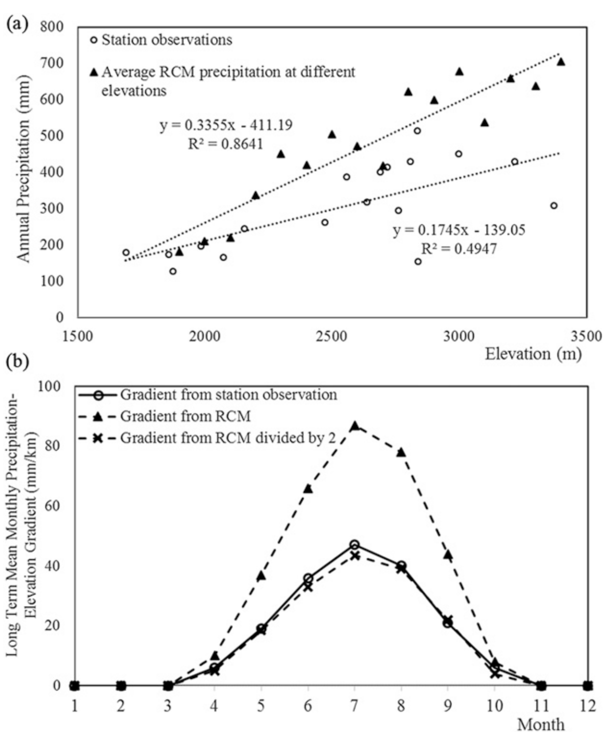


FIG. 4. Comparison of the mean precipitation–elevation gradients for the entire study area derived from the station observations and RCM output: (a) change of the precipitation with the elevation and (b) monthly precipitation–elevation gradients.

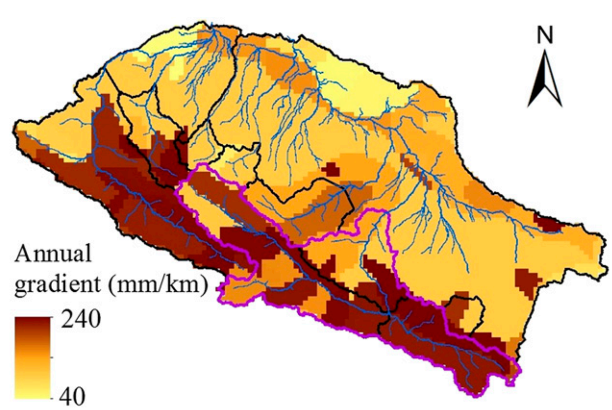


FIG. 6. The annual precipitation–elevation gradients in different facets.

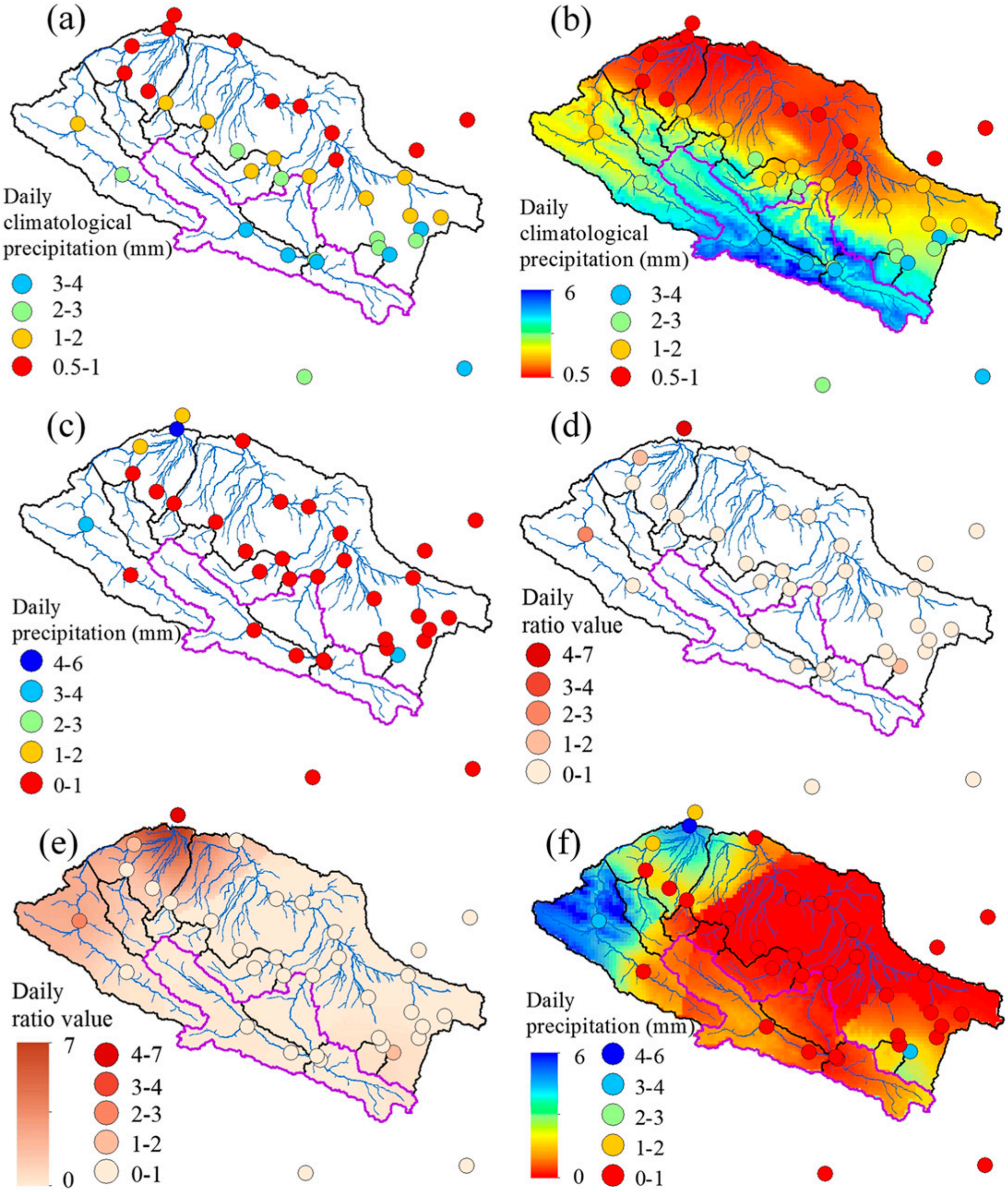


FIG. 7. Precipitation interpolation results (an example for 1 Jul 2014): (a) daily climatological precipitation at the stations, (b) gridded value of the daily climatological precipitation, (c) precipitation observed at stations, (d) ratio of daily observed precipitation to the climatological precipitation at the locations of the stations, (e) the gridded ratio of daily observed precipitation to the climatological precipitation, and (f) the interpolated daily grid precipitation.

(http://data.cma.cn). The hydrological stations observe hydrological elements, including river flow and water level, as well as precipitation and air temperature. Remarkably, most of the meteorological stations and hydrological stations are located in low-altitude areas, while only a few gauges are located in the mountainous areas (Fig. 2).

An experimental watershed, namely, the Hulugou watershed (Chen et al. 2013), is located at the northern slope of the mountain in the western tributary, close to the Zhamashike hydrological station (Fig. 2), with an elevation range of 2960–4800 m and a drainage area of approximately 25 km$^2$. In this watershed, meteorological and hydrological observations, including precipitation, atmospheric pressure, air temperature, relative humidity, sunshine hours, evaporation, soil temperature, and frozen soil depth, were recorded during the experimental

TABLE 1. Indicators to characterize the false alarm and miss rate.

| | Interpolation result | |
|---|---|---|
| Gauge observation | Precipitation | No precipitation |
| Precipitation | Hit | Miss |
| No precipitation | False alarm | Correct negative |

period (Chen et al. 2013). This research is supported by a major research plan, the Integrated Research on the Ecohydrological Processes of the Heihe River Basin, funded by the National Natural Science Foundation of China since 2010 (Cheng et al. 2014). In the Hulugou watershed, there are four precipitation stations located at different elevations (Chen et al. 2014). The precipitation–elevation gradient estimated in the Hulugou watershed was used for verification.

The station with an elevation of 2980 m is located at the outlet of the Hulugou experimental watershed. A 3-yr (2011–13) observation of the daily precipitation at this station is used for validation. Another meteorological station, namely, the Arou Sunny Slope station (see Fig. 2) with an elevation of 3529 m, was established in 2013 (Liu et al. 2011) by the Heihe Watershed Allied Telemetry Experimental Research (HiWATER; X. Li et al. 2013), which is a research project of the major research plan of Integrated Research on the Ecohydrological Processes of the Heihe River Basin. The daily precipitation recorded in 2014 at this station was also used for validation.

#### 2) PRECIPITATION DATA FROM AN RCM SIMULATION

RCMs were applied to the HRB in many previous studies (Gao et al. 2006; Liu et al. 2007), and some studies focused on precipitation simulations (Xiong and Yan 2013; Pan et al. 2015). Xiong and Yan (2013) constructed a 3-km-resolution RCM in the HRB based on Regional Integrated Environment Modeling System, version 2.0 (RIEMS2.0; Xiong et al. 2009). The dynamic core of the model was a no-hydrostatic version of the Fifth-generation Pennsylvania State University–NCAR Mesoscale Model (MM5); in addition, the RCM included the Biosphere–Atmosphere Transfer Scheme (BATS; Dickinson et al. 1993), the cumulus convective parameterization (Fritsch and Chappell 1980; Grell 1993), and the radiative transfer scheme used in the Community Climate Model, version 3 (CCM3; Kiehl et al. 1996). The observational and remotely sensed data are used to recalibrate the model's important parameters to gain a high spatial resolution to accurately simulate the precipitation. The vegetation types and distribution and the soil parameters were updated using the datasets provided by the Environmental and Ecological Science Data Center for West China, National Natural Science Foundation of China (http://westdc.westgis.ac.cn). The lateral boundary conditions for temperature, water vapor, wind, and surface pressure are extracted from the National Centers for Environmental Prediction Final (NCEP FNL) reanalysis data (Kalnay et al. 1996) with a spatial resolution of 1°. The lateral boundary conditions were provided via an exponential relaxation scheme. The simulated domain encompassed the entire HRB region, centered at 40.30°N, 99.50°E; the horizontal mesh consisted of 181 and 221 grid points in the longitudinal and latitudinal directions, respectively. A 3-km-resolution precipitation product for the HRB from 1980 to 2010 was generated based on the model, and the product was validated by the meteorological observations that had a high accuracy in simulating annual, seasonal, and daily precipitations at most of the grids where the gauges were located (Xiong and Yan 2013).

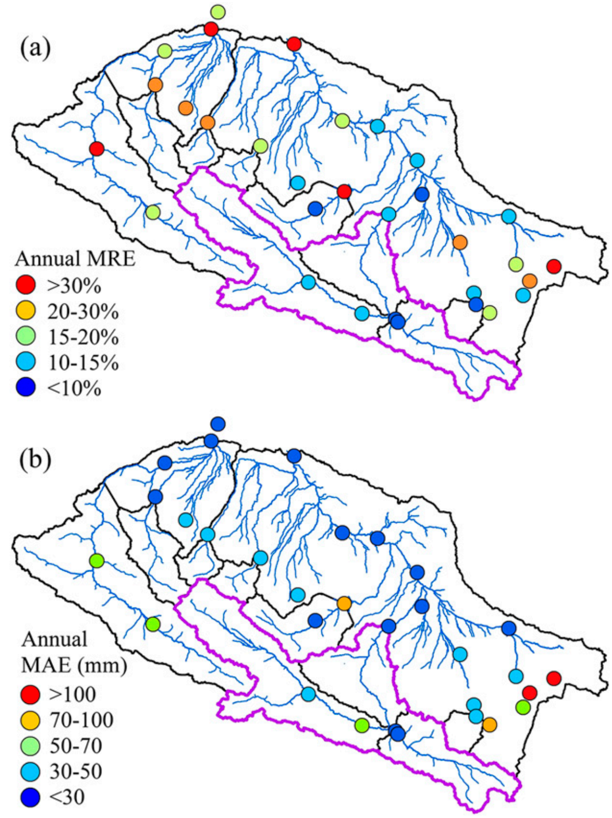


FIG. 8. GCV results: (a) annual MRE and (b) annual MAE.

### c. *Interpolation of the 3-km gridded daily precipitation data in HRB*

In the HRB, a DEM with the same resolution (3 km) and the same projection (Lambert conformal conic

TABLE 2. GCV results at each meteorological and hydrological station.

| Station name | $R^2$ for daily data | $R^2$ for monthly data | POD | FAR | EST |
|---|---|---|---|---|---|
| Jiuquan | 0.40 | 0.84 | 0.74 | 0.30 | 0.54 |
| Gaotai | 0.65 | 0.90 | 0.81 | 0.27 | 0.60 |
| Tuole | 0.42 | 0.70 | 0.64 | 0.28 | 0.45 |
| Yeniugou | 0.53 | 0.80 | 0.80 | 0.12 | 0.66 |
| Zhangye | 0.69 | 0.85 | 0.84 | 0.19 | 0.68 |
| Qilian (meteorological station) | 0.93 | 0.99 | 0.88 | 0.01 | 0.84 |
| Shandan | 0.60 | 0.83 | 0.81 | 0.21 | 0.63 |
| Gaoya | 0.64 | 0.90 | 0.89 | 0.09 | 0.79 |
| Sunan | 0.73 | 0.93 | 0.87 | 0.21 | 0.63 |
| Qilian (hydrological station) | 0.99 | 0.93 | 0.94 | 0.01 | 0.90 |
| Shuangshusi | 0.65 | 0.78 | 0.88 | 0.17 | 0.67 |
| Binggoutai | 0.50 | 0.83 | 0.88 | 0.33 | 0.52 |
| Yingluoxia | 0.59 | 0.89 | 0.85 | 0.05 | 0.78 |
| Yuanyangchi | 0.58 | 0.76 | 0.84 | 0.29 | 0.56 |
| Liqiao | 0.69 | 0.91 | 0.88 | 0.10 | 0.75 |
| Hongsihu | 0.77 | 0.74 | 0.84 | 0.12 | 0.68 |
| Pingchuan | 0.45 | 0.88 | 0.76 | 0.22 | 0.59 |
| Liuba | 0.67 | 0.84 | 0.89 | 0.11 | 0.76 |
| Liyuanbu | 0.72 | 0.91 | 0.89 | 0.27 | 0.61 |
| Xindi | 0.54 | 0.75 | 0.73 | 0.10 | 0.63 |
| Dahe | 0.49 | 0.64 | 0.80 | 0.17 | 0.62 |
| Hongshahe | 0.60 | 0.68 | 0.81 | 0.20 | 0.63 |
| Biandukou | 0.60 | 0.89 | 0.87 | 0.19 | 0.62 |
| Zhamashike | 0.67 | 0.94 | 0.90 | 0.09 | 0.76 |
| Zhengyixia | 0.55 | 0.77 | 0.87 | 0.19 | 0.70 |
| Hongshan | 0.39 | 0.70 | 0.76 | 0.28 | 0.55 |
| Dahuangshan | 0.72 | 0.72 | 0.82 | 0.17 | 0.63 |
| Xiakouyi | 0.51 | 0.77 | 0.89 | 0.29 | 0.59 |
| Fenglehe | 0.91 | 0.83 | 0.86 | 0.11 | 0.77 |
| Kangle | 0.32 | 0.55 | 0.73 | 0.22 | 0.53 |
| Maying | 0.62 | 0.84 | 0.91 | 0.48 | 0.45 |
| Zhulongguan | 0.40 | 0.60 | 0.65 | 0.57 | 0.29 |

projection) as the RCM is used in order to directly utilize the RCM output. Sixteen cycles of smooth processing of the DEM are selected after comparing other cycle numbers, and the facets are divided based on the smoothed terrain (Fig. 3). Then, the precipitation–elevation gradient is calculated in each facet.

There are a total of 18 precipitation observation sites (including meteorological and hydrological stations) in the mountain areas of the HRB, and these stations are distributed at elevations from 1700 to 3400 m. The annual precipitation–elevation gradient estimated from the stations is 170 mm km$^{-1}$ (see Fig. 4a) and 330 mm km$^{-1}$ estimated from the RCM output in the elevation range of 1700–3400 m (see Fig. 4b). Therefore, the precipitation–elevation gradients estimated from the RCM output for all facets are uniformly adjusted by the ratio of 170/330. Moreover, the precipitation–elevation gradient observed in the Hulugou experimental catchment is compared with the gradient from the RCM output, and a similar ratio is obtained (see Fig. 5).

Using the adjusted annual precipitation–elevation gradient shown in Fig. 6, the gridded daily precipitation climatology is generated using Eq. (5), and then the gridded ratio of daily precipitation to daily climatological precipitation is estimated using Eqs. (7)–(10). Finally, the daily gridded precipitation is generated using Eq. (11).

Figure 7 shows an example of generating the gridded precipitation on 1 July 2014. First, by combining the station's daily climatological precipitation on 1 July (Fig. 7a), the gridded climatological precipitation on 1 July (Fig. 7b) is generated using Eq. (2) based on the precipitation–elevation gradient given in Fig. 6 and the elevation given in Fig. 2. Then, based on the station precipitation on 1 July 2014 (Fig. 7c) and the gridded climatological precipitation, the ratios at the stations (Fig. 7d) are calculated and interpolated over the entire region (Fig. 7e). Multiplying the daily gridded climatological precipitation by the gridded ratio, the daily grid precipitation on 1 July 2014 is generated (Fig. 7f).

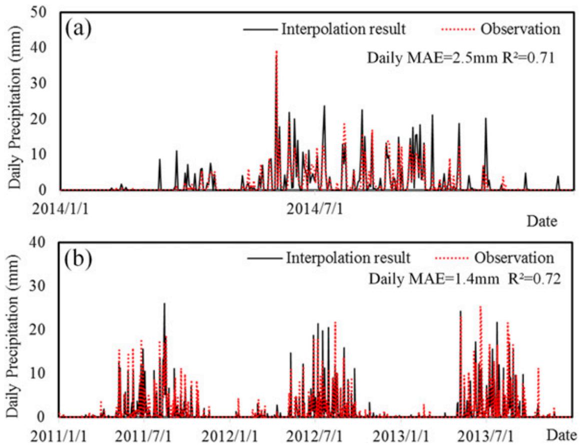


FIG. 9. Validation of daily interpolated precipitation based on experimental stations (a) the Arou Sunny Slope station in 2014 and (b) the Hulugou station from 2011 to 2013.

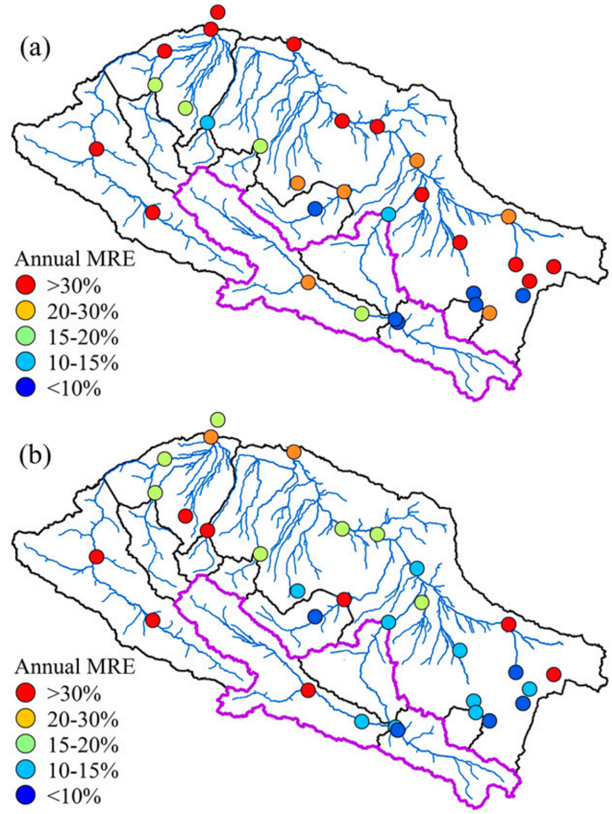


FIG. 10. Annual MRE of cross validation using (a) ADW method without considering the precipitation–elevation gradient and (b) ADW method considering the precipitation–elevation gradient estimated from the observations.

### *d. Evaluation methods and indices*

This study designs a GCV, which is commonly used for validating the interpolation results (Willmott and Matsuura 1995; Hofstra et al. 2008; New et al. 1999), to evaluate the interpolation method proposed in this study. The evaluating indices include mean absolute errors (MAE), mean relative errors (MRE), and $R^2$ for annual, monthly, and daily precipitation. Only the days with precipitation (either for the interpolation result or for the observed data) were selected to calculate daily MAE; the days with no precipitation were not used (Pan et al. 2015). In addition, the indices of probability of detection (POD), the false alarm rate (FAR), and the equitable threat score (ETS) are also adapted (Ebert et al. 2007; Shen and Xiong 2016). These indices can be calculated using the following equations:

$$\mathrm{POD} = \frac{H}{H+M}, \tag{12}$$

$$\mathrm{FAR} = \frac{F}{H+F}, \quad \text{and} \tag{13}$$

$$\mathrm{EST} = \frac{H-\mathrm{He}}{H+M+F-\mathrm{He}}, \tag{14}$$

where $\mathrm{He} = (H+M)(H+F)/(H+M+F+C)$ for hit $H$, miss $M$, false alarm $F$, and correct negative $C$ (see Table 1). POD represents the ratio of correctly identified precipitation values in all the observed precipitation values. FAR represents the ratio of precipitation that did not actually occur. The three indices range from 0 to 1. For POD and ETS, 0 is the worst score and 1 is the best score, while for FAR, 0 is the best and 1 is the worst. In the statistical process of the three indices, only the precipitation $\geq$0.1 mm day$^{-1}$ is used to ensure the reliability of the results.

To verify the reliability of the daily interpolation precipitation in the mountain areas, the interpolated daily precipitation is evaluated using two independent experimental stations (the Arou Sunny Slope and Hulugou stations) that are not used for interpolation. To examine the effect of precipitation–elevation information provided by the RCM output for the interpolation, two other interpolation methods are designed for comparison. One method is only using the ADW method without consideration of the precipitation–elevation relationship, and the other is using the ADW with the precipitation–elevation information based on the station (meteorological stations and hydrological stations). The values of MAE and MRE are calculated in the comparisons.

## 4. Results and discussion

### *a. Validation*

#### 1) CROSS VALIDATION

Figure 8 gives the annual MRE and MAE of the GCV results. The annual MRE at most stations is less than

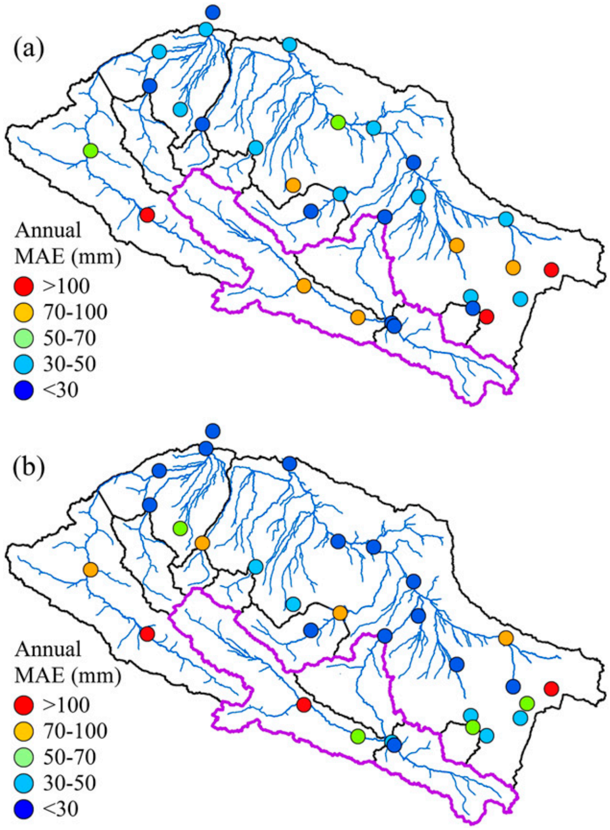


FIG. 11. Annual MAE of cross validation using (a) ADW method without considering the precipitation–elevation gradient and (b) ADW method considering the precipitation–elevation gradient estimated from the observations.

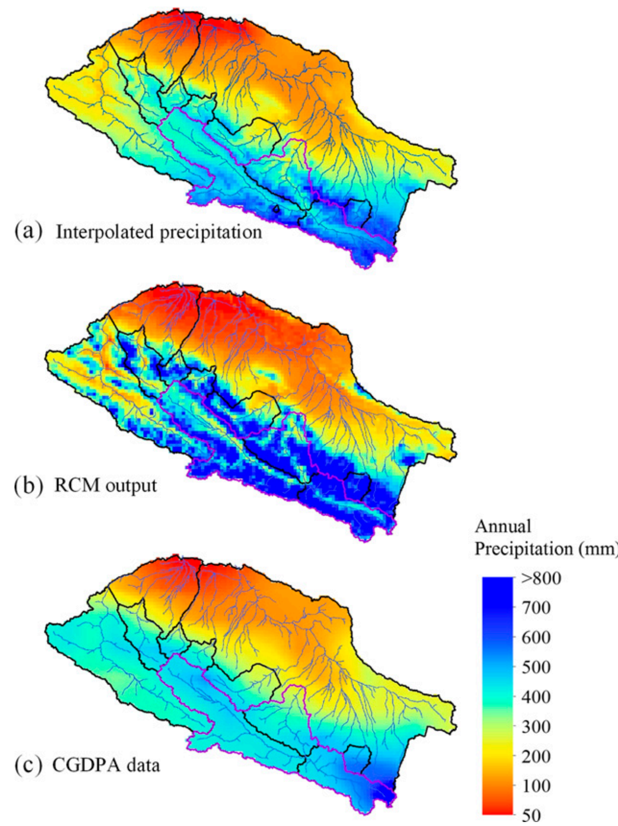


FIG. 12. Comparing the spatial distributions of the annual mean precipitation during the period 1980–2010: (a) interpolation result, (b) RCM output, and (c) CGDPA data (resampled into a 3-km grid).

30%, and the annual MAE at most stations is less than 50 mm. In the upper reach of the HRB, the annual MAE is less than 70 mm (MRE less than 15%), which is acceptable in mountainous areas.

Table 2 provides the other indices of the GCV results. The $R^2$ between the interpolated and observed precipitation values is larger than 0.4 for the daily data and is larger than 0.7 for the monthly precipitation. For most of the stations, the values of POD are larger than 0.7, the values of FAR are less than 0.3, and the values of ETS are larger than 0.5. These results indicate that the proposed method has reasonable accuracy.

### 2) VALIDATION USING INDEPENDENT OBSERVATIONS AT TWO EXPERIMENTAL STATIONS

This validation uses two independent stations that have not been used in the interpolation. Figure 9a shows the comparison between the interpolated and observed daily precipitation values at the Arou Sunny Slope station, in which the daily MAE are 2.5 mm and the $R^2$ is 0.71. The Arou Sunny Slope station lacks snowfall observations, and thus, the bias is large before April and after September. Figure 9b shows the comparison at the Hulugou station, where the daily MAE is 1.4 mm and the $R^2$ is 0.72. The independent validation results show that the daily precipitation interpolation results have sufficient accuracy.

## b. *Comparing the interpolation results with/without the precipitation–elevation relationship*

Figure 10a shows the result of the ADW interpolation without considering the precipitation–elevation relationship. Compared with the interpolation result shown in Fig. 8a, which is interpolated using the ADW method considering the precipitation–elevation obtained from RCM output and modified by the station observations, the interpolation result without consideration of the precipitation–elevation relationship has much larger relative errors at most stations. Figure 10b shows the result using the ADW interpolation and the precipitation–elevation relationship

TABLE 3. Mean annual water balance in different catchments from 2001 to 2010.

| | Annual precipitation (mm) | | | Annual total of runoff and actual evapotranspiration (mm) |
|---|---|---|---|---|
| | Present method | CGDPA | RCM | |
| Upper catchment (Yingluoxia hydrological station) | 488 | 474 | 700 | 485 |
| West catchment of the upper reach (Zhamashike hydrological station) | 491 | 477 | 641 | 469 |
| East catchment of the upper reach (Qilian hydrological station) | 531 | 526 | 795 | 526 |
| Hongshui River catchment (Shuangshusi hydrological station) | 580 | 536 | 814 | 487 |
| Liyuan River catchment (Liyuanbu hydrological station) | 396 | 400 | 492 | 275 |
| Maying River catchment (Hongshahe hydrological station) | 430 | 410 | 538 | 359 |
| Fengle River catchment (Fenglehe hydrological station) | 386 | 423 | 552 | 352 |
| Hongshui River catchment (Xindi hydrological station) | 393 | 425 | 453 | 313 |
| Taolai River catchment (Binggou hydrological station) | 336 | 430 | 375 | 282 |

obtained from the station observations. This result is better than that without considering the precipitation–elevation relationship shown in Fig. 10a, indicating that the precipitation–elevation relationship is useful for the spatial interpolation of precipitation. However, at most stations, the result is worse than the result shown in Fig. 8a, indicating that the RCM output can provide useful precipitation–elevation information to improve the spatial interpolation of precipitation, especially in the sparsely gauged or ungauged area.

Figure 11 shows the annual MAE result of GCV, which is similar to the annual MRE result, and it is more obvious that in the mountain areas, the interpolated result using the precipitation–elevation relationship provided by RCM output can effectively reduce the MAE in the high elevation areas, such as the Tuole, Yeniugou, and Zhamashike stations.

### c. *Rationality evaluation of the interpolated precipitation*

Figure 12 compares the spatial distributions of the interpolated precipitation, the CGDPA product (Shen and Xiong 2016), and the RCM output. These three types of precipitation data captured the major characteristics of the precipitation distribution in HRB in which the precipitation diminishes from the south to the north. However, there are two major differences among the spatial distributions of the three precipitation products. First, the precipitation amounts derived from interpolated precipitation and CGDPA in the upper HRB mountainous areas are similar, while the precipitation derived from the RCM output is much larger. Second, the interpolation result and the RCM output, in the mountain areas, clearly show that the precipitation is higher in the eastern region than in the western region. The CGDPA data could not show much difference between the eastern and the western regions of the upper HRB.

Since the sparse stations in the study area are not enough to validate the interpolated precipitation, the catchment water balance is used to analyze the rationality of the interpolated precipitation. The Integrated Research on the Ecohydrological Processes of the Heihe River Basin program developed a set of actual evapotranspiration data based on remote sensing from 2001 to 2012 (Wu et al. 2012; Wu 2013; http://westdc.westgis.ac.cn/). The ET data are validated in this region based on several flux towers' observation developed by the HiWATER project. The river discharge records at the hydrological stations are used to calculate the annual runoff of the catchments. Since the glacier melting runoff is very limited in HRB (Wang et al. 2015), the annual precipitation should be close to the sum of annual runoff and annual actual evapotranspiration. Table 3 shows the comparison of the catchment-averaged annual precipitation estimated from three datasets with the sum of annual actual evapotranspiration and runoff depth. In the upper HRB (upstream of the Yingluoxia station), the precipitation derived from the interpolation result and CGDPA data is close to the sum of actual evapotranspiration and runoff depth. The interpolated precipitation value is slightly higher in the western tributary. The precipitation derived from the RCM output is much larger than the sum of actual evapotranspiration and runoff depth.

TABLE 4. Comparison of the decadal mean of annual precipitation (obtained in this study and from the CGDPA dataset) and annual runoff depth.

| Precipitation/runoff (mm $yr^{-1}$) | 1960s | 1970s | 1980s | 1990s | After 2000 |
|---|---|---|---|---|---|
| Upper catchment (Yingluoxia hydrological station) | | | | | |
| This study | 349 | 376 | 474 | 458 | 484 |
| CGDPA | 424 | 435 | 456 | 433 | 480 |
| Runoff depth | 147 | 139 | 174 | 158 | 181 |
| West catchment in the upper reach (Zhamashike hydrological station) | | | | | |
| This study | 320 | 344 | 470 | 448 | 487 |
| CGDPA | 412 | 431 | 454 | 421 | 484 |
| Runoff depth | 142 | 132 | 148 | 140 | 169 |
| East catchment in upper reach (Qilian hydrological station) | | | | | |
| This study | 405 | 436 | 522 | 513 | 527 |
| CGDPA | 498 | 489 | 516 | 507 | 530 |
| Runoff depth | 213 | 155 | 196 | 180 | 196 |
| Liyuan River catchment (Liyuanbu hydrological station) | | | | | |
| This study | 294 | 328 | 370 | 372 | 398 |
| CGDPA | 339 | 382 | 373 | 360 | 397 |
| Runoff depth | 112 | 110 | 131 | 113 | 133 |
| Hongshui River catchment (Xindi hydrological station) | | | | | |
| This study | 244 | 274 | 378 | 349 | 386 |
| CGDPA | 356 | 378 | 404 | 354 | 430 |
| Runoff depth | 151 | 152 | 142 | 153 | 159 |
| Taolai River catchment (Binggou hydrological station) | | | | | |
| This study | 188 | 215 | 334 | 286 | 328 |
| CGDPA | 353 | 377 | 404 | 355 | 436 |
| Runoff depth | 87 | 97 | 90 | 82 | — |
| Fengle River catchment (Fenglehe hydrological station) | | | | | |
| This study | 246 | 277 | 358 | 360 | 381 |
| CGDPA | 352 | 377 | 397 | 357 | 426 |
| Runoff depth | 121 | 137 | 159 | 168 | 174 |
| Maying River catchment (Hongshahe hydrological station) | | | | | |
| This study | 271 | 306 | 399 | 400 | 423 |
| CGDPA | 344 | 382 | 381 | 358 | 413 |
| Runoff depth | 183 | 179 | 169 | 175 | 177 |
| Hongshui River catchment (Shuangshusi hydrological station) | | | | | |
| This study | 445 | 527 | 552 | 530 | 560 |
| CGDPA | 479 | 496 | 504 | 504 | 530 |
| Runoff depth | 235 | 214 | 248 | 192 | 218 |

In the western part of the study area, the long-term mean annual values of the interpolated precipitation in the Taolai River watershed (upstream of the Binggou station) and the Hongshui River watershed (upstream of the Xindi station) are 336 and 393 mm, respectively. The long-term mean CGDPA precipitation is 430 mm for the Taolai River watershed and 425 mm for the Hongshui River watershed. The long-term mean value of the sum of actual evapotranspiration and runoff in the two watersheds is 282 mm for the Taolai River watershed and 313 mm for the Hongshui River watershed, which are closer to the interpolated precipitation values. This result indicates that the interpolated precipitation is more reasonable than CGDPA data in terms of the watershed water balance.

Table 4 compares the annual precipitation derived from the interpolation result and CGDPA data in different subbasins. In the 1960s and 1970s, the precipitation derived from the interpolation result is generally less than that from CGDPA data. This result is probably because in the 1960s and 1970s, there were few hydrological stations, and the snow observation technique was poor. In the Fengle River watershed and the Maying River watershed, the interpolated precipitation slightly increased from the 1980s to the 1990s (from 358 to 360 mm in the Fengle River watershed and from 399 to 400 mm in the Maying River watershed), while the CGDPA precipitation showed a significant decreasing trend (from 397 to 357 mm in the Fengle River watershed and from 381 to 358 mm in the Maying River watershed). The runoff depth from the hydrological observations in these two decades showed an increasing trend (from 159 to 168 mm in the Fengle River watershed and from 169 to 175 mm in the Maying River

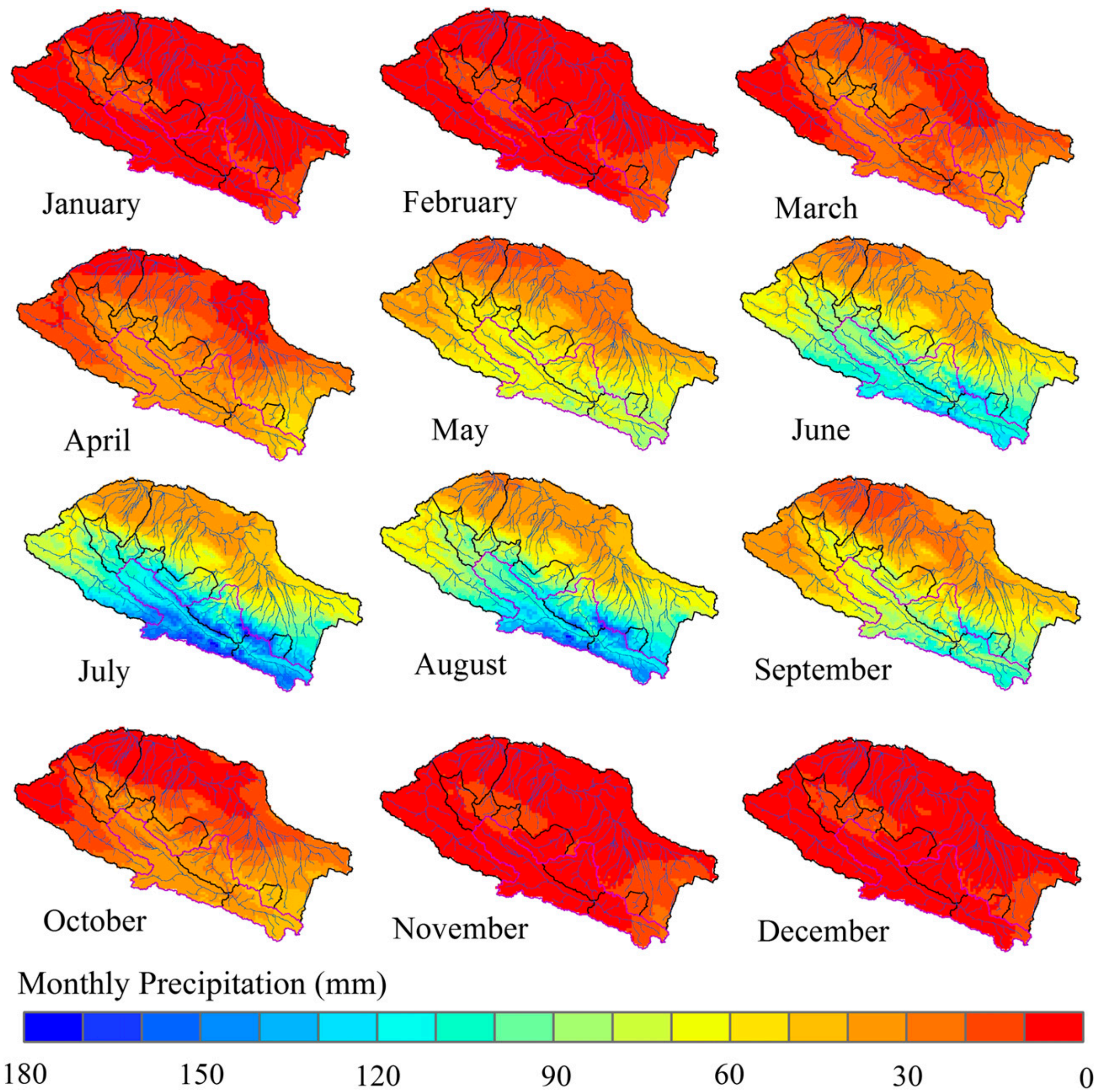


FIG. 13. Spatial distributions of the mean monthly precipitation in the period of 1980–2014 obtained in this study.

watershed). Therefore, we can confirm that the interpolated precipitation is more reliable for the two watersheds.

Figure 13 shows the spatial distribution of the long-term mean monthly value of the interpolated precipitation from 1980 to 2014 in the upper and middle reaches of the HRB. The precipitation is very low in winter, which falls as snow in the region of the Fengle River watershed and the Maying River watershed. The major rainy season is from May to September, and most rainfall is distributed in the upper mountain areas. The spatiotemporal distribution of precipitation provided by the interpolation data is important for understanding and modeling the regional ecohydrology.

### d. *Uncertainties of the interpolated precipitation*

There are some uncertainties in the interpolation processes. As mentioned in section 3c, because the stations in the mountains are distributed in the elevation range of 1700–3400 m, the bias of RCM is adjusted by the ratio that is obtained in the same elevation range. We assume that this ratio suits the entire study area (in the elevation range of 800–5500 m, see Fig. 2). This assumption may cause uncertainties, which need further study based on extra precipitation observations at the higher elevation.

In addition, more attention should be paid to uncertainty from the RCM simulation. Besides the systematic bias discussed above, differences between the simulated results from different RCMs can be found. For example, the precipitation–elevation gradient derived from the RCM simulation used in this study has some differences in comparison to the gradient derived from another high-spatial-resolution RCM simulation (Pan et al. 2015). The accuracy of the RCM simulation result has an important effect on the reliability of the interpolated precipitation. Therefore, it is necessary to explore the way to reduce the uncertainty in the precipitation outputted by RCM, and ensemble estimation from multi-RCMs is a possible choice in the future studies. Certainly, the future improvement of RCMs will be of great benefit to reduce the uncertainty.

## 5. Conclusions

This study proposed a spatial interpolation method for daily precipitation, which combines gauge observations and RCM output. Application of this method in the upper and middle reaches of the Heihe River basin produced 3-km-resolution gridded precipitation data from 1960 to 2014 based on 25 hydrological stations and 15 national meteorological stations, along with the RCM output. The following conclusions can be drawn from the results presented in this study.

1) The precipitation interpolation method that considers the precipitation–elevation relationship derived from the RCM output is effective for generating high-spatial-resolution precipitation data based on sparse observation stations.
2) Based on the generalized cross validation results, the annual MRE at most stations is less than 30%, and the annual MAE is less than 50 mm. The monthly $R^2$ at most stations is larger than 0.7. Independent validation based on the observation at the Hulugou station and the Arou Sunny Slope station shows that the daily interpolated precipitation has high accuracy, with the daily $R^2$ larger than 70%. These results indicate that the interpolation method is reliable and has sufficient accuracy.
3) A comparison between the interpolation results with/without the RCM output shows the RCM output provides useful information of the precipitation spatial pattern, which can be used to generate high-spatial-resolution precipitation data with a limited number of precipitation observations.

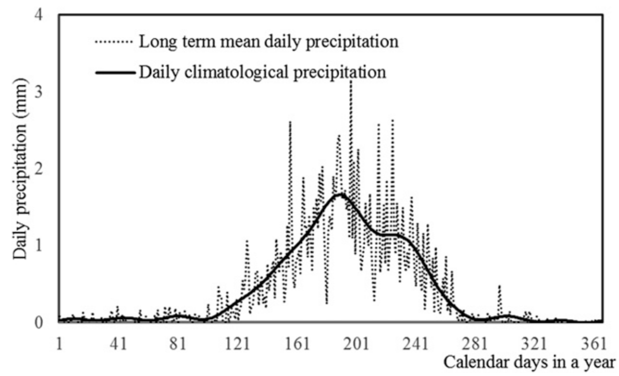


FIG. A1. An example of estimating the daily climatological precipitation at the stations.

4) This precipitation interpolation method is especially important for ecohydrological studies in the watersheds located in high mountainous areas where the meteorological stations are usually very sparse and the precipitation varies with elevation.

However, a few limitations remain in the current study. Since the precipitation distribution is very complex, especially in mountainous areas, it could not be simply explained using the elevation gradient. The effects of other factors on the spatial distribution of precipitation will be considered in future studies.

*Acknowledgments.* This research was supported by the major research plan entitled, ''Integrated Research on the Ecohydrological Processes of the Heihe River Basin'' (Grants 91225302 and 91425303) funded by the national Natural Science Foundation of China (NSFC), the project of public science and technology research funded by the Ministry of Water Resources of China (Grant 201401008), and the National Program for Support of Top-notch Young Professionals. The authors thank three anonymous reviewers and the editors for their constructive comments, which greatly improved the manuscript.

## APPENDIX

### Method of Generating the Gridded Daily Climatological Precipitation

Figure A1 shows an example of generating the daily climatological precipitation at a station. The dotted line in this figure shows the long-term mean daily precipitation for 365 calendar days. It is clear that high-frequency noise exists. To obtain a smooth curve of

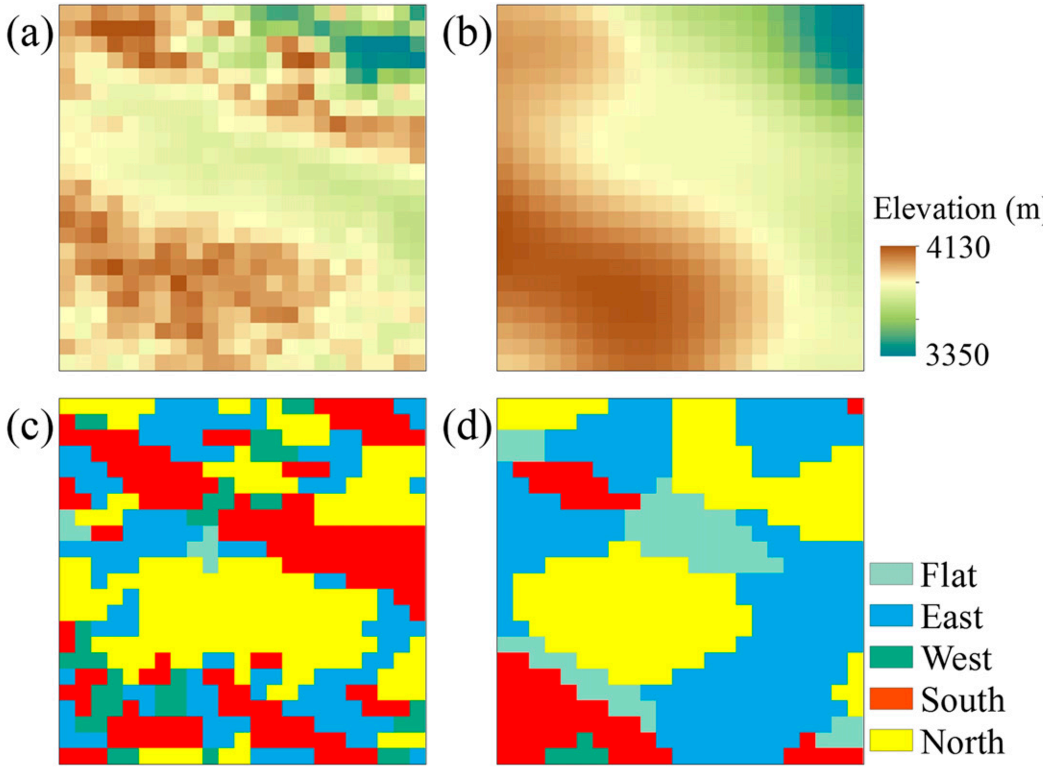


FIG. A2. Sketch map of generating the facets: (a) original DEM without smooth processing, (b) smoothed DEM after 40 cycles of smooth processing, (c) major orientation of each grid cell based on the original DEM, and (d) major orientation of each grid cell based on the smoothed DEM.

the climatological precipitation, a Fourier filtering process is used to remove the high-frequency noise. The filtering result is the daily climatological precipitation, which maintains the major changing trend only (see the solid line in the figure).

Figure A2 is a sketch map for generating the facets. This figure compares an original DEM without smooth processing (Fig. A2a) with a highly smoothed terrain after 40 times of smoothing cycle (Fig. A2b), as well as the facets derived from the two DEMs. The major orientation (east, south, west, north, or flat) of each grid cell is determined by the slope gradients in the four directions. The results are shown in Figs. A2c and A2d. A facet is composed of adjacent grid cells that have the same orientation. The smooth processing reduces the number of facets, meanwhile increasing the average area (number of grid cells) of each facet. Since the precipitation–elevation gradient is estimated using a regression analysis in each facet, a facet should contain a sufficient number of grid cells. The minimum number of grid cells for one facet is five in this study. An appropriate smoothing processing should reduce the number of the facets containing five or fewer grid cells.

## REFERENCES

Basist, A., G. D. Bell, and V. Meentemeyer, 1994: Statistical relationships between topography and precipitation patterns. *J. Climate*, **7**, 1305–1315, doi:10.1175/1520-0442(1994)007<1305:SRBTAP>2.0.CO;2.

Berne, A., and W. F. Krajewski, 2013: Radar for hydrology: Unfulfilled promise or unrecognized potential? *Adv. Water Resour.*, **51**, 357–366, doi:10.1016/j.advwatres.2012.05.005.

Chen, R. S., C. T. Han, Y. X. Song, and J. F. Liu, 2013: Manual observation of meteorological data in Hulugou sub-basin of Heihe River basin. Heihe Plan Science Data Center, accessed 25 November 2016, doi:10.3972/heihe.073.2013.db.

——, Y. X. Song, E. S. Kang, C. T. Han, J. F. Liu, Y. Yang, W. W. Qing, and Z. W. Liu, 2014: A cryosphere–hydrology observation system in a small alpine watershed in the Qilian Mountains of China and its meteorological gradient. *Arct. Antarct. Alp. Res.*, **46**, 505–523, doi:10.1657/1938-4246-46.2.505.

Cheng, G. D., X. Li, and W. Z. Zhao, 2014: Integrated study of the water–ecosystem–economy in the Heihe River basin. *Natl. Sci. Rev.*, **1**, 413–428, doi:10.1093/nsr/nwu017.

Daly, C., R. P. Neilson, and D. L. Phillips, 1994: A statistical–topographic model for mapping climatological precipitation over mountainous terrain. *J. Appl. Meteor.*, **33**, 140–158, doi:10.1175/1520-0450(1994)033<0140:ASTMFM>2.0.CO;2.

——, M. Halbleib, J. I. Smith, W. P. Gibson, M. K. Doggett, G. H. Taylor, J. Curtis, and P. P. Pasteris, 2008: Physiographically sensitive mapping of climatological temperature and precipitation across the conterminous United States. *Int. J. Climatol.*, **28**, 2031–2064, doi:10.1002/joc.1688.

Diallo, I., M. B. Sylla, F. Giorgi, A. T. Gaye, and M. Camara, 2012: Multimodel GCM–RCM ensemble-based projections of temperature and precipitation over West Africa for the early 21st century. *Int. J. Geophys.*, **2012**, 1–19, doi:10.1155/2012/972896.

Dickinson, R. E., M. Errico, F. Giorgi, and G. T. Bates, 1989: A regional climate model for the western United States. *Climatic Change*, **15**, 383–422, doi:10.1007/BF00240465.

——, A. Henderson-Sellers, and P. J. Kennedy, 1993: Biosphere–Atmosphere Transfer Scheme (BATS) Version 1e as coupled to the NCAR Community Climate Model. NCAR Tech. Note NCAR/TN-387+STR, 88 pp., doi:10.5065/D67W6959.

Ding, Y., B. Ye, and W. Zhou, 1999: Temporal and spatial precipitation distribution in the Heihe catchment, northwest China, during the past 40a (in Chinese). *J. Glaciol. Geocryology*, **1**, 42–48.

Ebert, E. E., J. E. Janowiak, and C. Kidd, 2007: Comparison of near-real-time precipitation estimates from satellite observations and numerical models. *Bull. Amer. Meteor. Soc.*, **88**, 47–64, doi:10.1175/BAMS-88-1-47.

Feldmann, H., G. Schädler, H. J. Panitz, and C. Kottmeier, 2013: Near future changes of extreme precipitation over complex terrain in central Europe derived from high resolution RCM ensemble simulations. *Int. J. Climatol.*, **33**, 1964–1977, doi:10.1002/joc.3564.

Fritsch, J. M., and C. F. Chappell, 1980: Numerical prediction of convectively driven mesoscale pressure systems. Part I: Convective parameterization. *J. Atmos. Sci.*, **37**, 1722–1733, doi:10.1175/1520-0469(1980)037<1722:NPOCDM>2.0.CO;2.

Gao, B., Y. Qin, Y. H. Wang, D. W. Yang, and Y. R. Zheng, 2016: Modeling ecohydrological processes and spatial patterns in the upper Heihe basin in China. *Forests*, **7**, 10, doi:10.3390/f7010010.

Gao, Y. H., G. D. Cheng, W. R. Cui, F. Chen, D. Gochis, and W. Yu, 2006: Coupling of enhanced land surface hydrology with atmospheric mesoscale model and its implement in the Heihe River basin (in Chinese). *Adv. Earth Sci.*, **21**, 1283–1292.

Giorgi, F., and G. T. Bates, 1989: The climatological skill of a regional model over complex terrain. *Mon. Wea. Rev.*, **117**, 2325–2347, doi:10.1175/1520-0493(1989)117<2325:TCSOAR>2.0.CO;2.

Grell, G. A., 1993: Prognostic evaluation of assumptions used by cumulus parameterizations. *Mon. Wea. Rev.*, **121**, 764–787, doi:10.1175/1520-0493(1993)121<0764:PEOAUB>2.0.CO;2.

Hofstra, N., M. Haylock, M. New, P. Jones, and C. Frei, 2008: Comparison of six methods for the interpolation of daily European climate data. *J. Geophys. Res.*, **113**, 6089–6098, doi:10.1029/2008JD010100.

Huffman, G. J., and Coauthors, 2007: The TRMM Multisatellite Precipitation Analysis (TMPA): Quasi-global, multiyear, combined-sensor precipitation estimates at fine scales. *J. Hydrometeor.*, **8**, 38–55, doi:10.1175/JHM560.1.

Hutchinson, M. F., 1995: Interpolating mean rainfall using thin plate smoothing splines. *Int. J. Geogr. Inf. Sys.*, **9**, 385–403, doi:10.1080/02693799508902045.

Jarvis, A., H. I. Reuter, A. Nelson, and E. Guevara, 2008: Hole-filled SRTM for the globe version 4. CGIAR-CSI SRTM 90m Database, accessed 25 November 2016. [Available online at http://www.cgiar-csi.org/data/srtm-90m-digital-elevation-database-v4-1.]

Joyce, R. J., J. E. Janowiak, P. A. Arkin, and P. Xie, 2004: CMORPH: A method that produces global precipitation estimates from passive microwave and infrared data at high spatial and temporal resolution. *J. Hydrometeor.*, **5**, 487–503, doi:10.1175/1525-7541(2004)005<0487:CAMTPG>2.0.CO;2.

Kalnay, E., and Coauthors, 1996: The NCEP/NCAR 40-Year Reanalysis Project. *Bull. Amer. Meteor. Soc.*, **77**, 437–472, doi:10.1175/1520-0477(1996)077<0437:TNYRP>2.0.CO;2.

Kaptué, A. T., N. P. Hanan, L. Prihodko, and J. A. Ramirez, 2015: Spatial and temporal characteristics of rainfall in Africa: Summary statistics for temporal downscaling. *Water Resour. Res.*, **51**, 2668–2679, doi:10.1002/2014WR015918.

Kiehl, J. T., J. J. Hack, G. B. Bonan, B. A. Boville, B. P. Briegleb, D. L. Williamson, and P. J. Rasch, 1996: Description of the NCAR Community Climate Model (CCM3). NCAR Tech. Note NCAR/TN-420+STR, 152 pp., doi:10.5065/D6FF3Q99.

Laux, P., S. Vogl, W. Qiu, H. R. Knoche, and H. Kunstmann, 2011: Copula-based statistical refinement of precipitation in RCM simulations over complex terrain. *Hydrol. Earth Syst. Sci.*, **15**, 2401–2419, doi:10.5194/hess-15-2401-2011.

Li, X., and Coauthors, 2013: Heihe Watershed Allied Telemetry Experimental Research (HiWATER): Scientific objectives and experimental design. *Bull. Amer. Meteor. Soc.*, **94**, 1145–1160, doi:10.1175/BAMS-D-12-00154.1.

Li, Z., D. W. Yang, and Y. Hong, 2013: Multi-scale evaluation of high-resolution multi-sensor blended global precipitation products over the Yangtze River. *J. Hydrol.*, **500**, 157–169, doi:10.1016/j.jhydrol.2013.07.023.

——, ——, ——, J. Zhang, and Y. C. Qi, 2014: Characterizing spatiotemporal variations of hourly rainfall by gauge and radar in the mountainous Three Gorges region. *J. Appl. Meteor. Climatol.*, **53**, 873–889, doi:10.1175/JAMC-D-13-0277.1.

Liang, X. Z., L. Li, K. E. Kunkel, M. Ting, and J. X. L. Wang, 2004: Regional climate model simulation of U.S. precipitation during 1982–2002. Part I: Annual cycle. *J. Climate*, **17**, 3510–3529, doi:10.1175/1520-0442(2004)017<3510:RCMSOU>2.0.CO;2.

Liu, S. M., Z. W. Xu, W. Z. Wang, Z. Z. Jia, M. J. Zhu, J. Bai, and J. M. Wang, 2011: A comparison of eddy-covariance and large aperture scintillometer measurements with respect to the energy balance closure problem. *Hydrol. Earth Syst. Sci.*, **15**, 1291–1306, doi:10.5194/hess-15-1291-2011.

Liu, W., G. D. Cheng, H. Y. Li, Y. H. Ran, G. D. Cheng, and F. Chen, 2007: Land use pattern of Heihe River basin and its impact modeling (in Chinese). *Plateau Meteor.*, **26**, 278–285.

Lloyd, C. D., 2005: Assessing the effect of integrating elevation data into the estimation of monthly precipitation in Great Britain. *J. Hydrol.*, **308**, 128–150, doi:10.1016/j.jhydrol.2004.10.026.

Maraun, D., and M. Widmann, 2015: The representation of location by regional climate models in complex terrain. *Hydrol. Earth Syst. Sci.*, **19**, 3449–3456, doi:10.5194/hess-19-3449-2015.

Maurya, R. K. S., and G. P. Singh, 2016: Simulation of present-day precipitation over India using a regional climate model. *Meteor. Atmos. Phys.*, **128**, 211–228, doi:10.1007/s00703-015-0409-x.

New, M., M. Hulme, and P. Jones, 1999: Representing twentieth-century space–time climate variability. Part I: Development of a 1961–90 mean monthly terrestrial climatology. *J. Climate*, **12**, 829–856, doi:10.1175/1520-0442(1999)012<0829:RTCSTC>2.0.CO;2.

——, ——, and ——, 2000: Representing twentieth-century space–time climate variability. Part II: Development of 1901–96 monthly grids of terrestrial surface climate. *J. Climate*, **13**, 2217–2238, doi:10.1175/1520-0442(2000)013<2217:RTCSTC>2.0.CO;2.

Nykanen, D. K., E. Foufoula-Georgiou, and W. M. Lapenta, 2001: Impact of small-scale rainfall variability on larger-scale spatial organization of land–atmosphere fluxes. *J. Hydrometeor.*, **2**, 105–121, doi:10.1175/1525-7541(2001)002<0105:IOSSRV>2.0.CO;2.

Pan, X. D., X. Li, G. D. Cheng, H. Li, and X. He, 2015: Development and evaluation of a river-basin-scale high spatio-temporal precipitation data set using the WRF Model: A case study of the Heihe River basin. *Remote Sens.*, **7**, 9230–9252, doi:10.3390/rs70709230.

Phillips, D. L., J. Dolph, and D. Marks, 1992: A comparison of geostatistical procedures for spatial analysis of precipitation in mountainous terrain. *Agric. For. Meteor.*, **58**, 119–141, doi:10.1016/0168-1923(92)90114-J.

Sanberg, J. A. M., and J. Oerlemans, 1983: Modeling of Pleistocene European ice sheets: The effect of upslope precipitation. *Geol. Mijnbouw*, **62**, 267–273.

Shen, Y., and A. Xiong, 2016: Validation and comparison of a new gauge-based precipitation analysis over mainland China. *Int. J. Climatol.*, **36**, 252–265, doi:10.1002/joc.4341.

Shepard, D., 1968: A two-dimensional interpolation function for irregularly spaced data. *Proc. 23rd National Conf. of the Association for Computing Machinery*, ACM, 517–524, doi:10.1145/800186.810616.

Tabios, G. Q., and J. D. Salas, 1985: A comparative analysis of techniques for spatial interpolation of precipitation. *J. Amer. Water Resour. Assoc.*, **21**, 365–380, doi:10.1111/j.1752-1688.1985.tb00147.x.

Taylor, C. M., R. J. Harding, A. J. Thorpe, and P. Bessemoulin, 1997: A mesoscale simulation of land surface heterogeneity from HAPEX-Sahel. *J. Hydrol.*, **188–189**, 1040–1066, doi:10.1016/S0022-1694(96)03182-4.

Thiessen, A. H., 1911: Precipitation averages for large areas. *Mon. Wea. Rev.*, **39**, 1082–1084, doi:10.1175/1520-0493(1911)39<1248a:DNGB>2.0.CO;2.

Wang, Y., D. Yang, H. Lei, and H. Yang, 2015: Impact of cryosphere hydrological processes on the river runoff in the upper reaches of Heihe River (in Chinese). *J. Hydraul. Eng.*, **46**, 1064–1071.

Willmott, C. J., and K. Matsuura, 1995: Smart interpolation of annually averaged air temperature in the United States. *J. Appl. Meteor.*, **34**, 2577–2586, doi:10.1175/1520-0450(1995)034<2577:SIOAAA>2.0.CO;2.

——, C. M. Rowe, and W. D. Philpot, 1985: Small-scale climate maps: A sensitivity analysis of some common assumptions associated with grid point interpolation and contouring. *Amer. Cartogr.*, **12**, 5–16.

Wu, B. F., 2013: Monthly evapotranspiration datasets (2000–2012) with 1 km spatial resolution over the Heihe River basin. Heihe Plan Science Data Center, accessed 25 November 2016, doi:10.3972/heihe.115.2013.db.

——, N. N. Yan, J. Xiong, W. G. M. Bastiaanssen, W. Zhu, and A. Stein, 2012: Validation of ETWatch using field measurements at diverse landscapes: A case study in Hai basin of China. *J. Hydrol.*, **436–437**, 67–80, doi:10.1016/j.jhydrol.2012.02.043.

Xie, P., M. Chen, S. Yang, A. Yatagai, T. Hayasaka, Y. Fukushima, and C. Liu, 2007: A gauge-based analysis of daily precipitation over East Asia. *J. Hydrometeor.*, **8**, 607–626, doi:10.1175/JHM583.1.

Xiong, Z., and X. D. Yan, 2013: Building a high-resolution regional climate model for the Heihe River basin and simulating precipitation over this region. *Chin. Sci. Bull.*, **58**, 4670–4678, doi:10.1007/s11434-013-5971-3.

——, C. B. Fu, and X. D. Yan, 2009: Regional integrated environmental model system and its simulation of East Asia summer monsoon. *Chin. Sci. Bull.*, **54**, 4253–4261, doi:10.1007/s11434-009-0669-2.

Yang, D. W., C. Li, G. H. Ni, and H. P. Hu, 2004: Application of a distributed hydrological model to the Yellow River basin. *Acta Geogr. Sin.*, **59**, 143–154.

——, B. Gao, Y. Jiao, H. M. Lei, Y. L. Zhang, H. B. Yang, and Z. T. Cong, 2015: A distributed scheme developed for eco-hydrological modeling in the upper Heihe River. *Sci. China Earth Sci.*, **58**, 36–45, doi:10.1007/s11430-014-5029-7.

Young, C. B., B. R. Nelson, A. A. Bradley, J. A. Smith, C. D. Peters-Lidard, A. Kruger, and M. L. Baeck, 1999: An evaluation of NEXRAD precipitation estimates in complex terrain. *J. Geophys. Res.*, **104**, 19 691–19 703, doi:10.1029/1999JD900123.